



## Article

# Evaluation of Spatiotemporal Resilience and Resistance of Global Vegetation Responses to Climate Change

Na Sun <sup>1,2,†</sup> , Naijing Liu <sup>1,2,†</sup> , Xiang Zhao <sup>1,2,\*</sup> , Jiacheng Zhao <sup>1,2</sup> , Haoyu Wang <sup>3</sup> and Donghai Wu <sup>4</sup>

<sup>1</sup> State Key Laboratory of Remote Sensing Science, Jointly Sponsored by Beijing Normal University and Aerospace Information Research Institute of Chinese Academy of Sciences, Faculty of Geographical Science, Beijing Normal University, Beijing 100875, China

<sup>2</sup> Beijing Engineering Research Center for Global Land Remote Sensing Products, Institute of Remote Sensing Science and Engineering, Faculty of Geographical Science, Beijing Normal University, Beijing 100875, China

<sup>3</sup> School of Earth and Space Sciences, Peking University, Beijing 100871, China

<sup>4</sup> Department of Ecology and Evolutionary Biology, Cornell University, Ithaca, NY 14853, USA

\* Correspondence: zhaoxiang@bnu.edu.cn; Tel.: +86-010-5880-0181

† These authors contributed equally to this work.

**Abstract:** The quantitative assessment of vegetation resilience and resistance is worthwhile to deeply understand the responses of vegetation growth to climate anomalies. However, few studies comprehensively evaluate the spatiotemporal resilience and resistance of global vegetation responses to climate change (i.e., temperature, precipitation, and radiation). Furthermore, although ecosystem models are widely used to simulate global vegetation dynamics, it is still not clear whether ecosystem models can capture observation-based vegetation resilience and resistance. In this study, based on remotely sensed and model-simulated leaf area index (LAI) time series and climate datasets, we quantified spatial patterns and temporal changes in vegetation resilience and resistance from 1982–2015. The results reveal clear spatial patterns of observation-based vegetation resilience and resistance for the last three decades, which were closely related to the local environment. In general, most of the ecosystem models capture spatial patterns of vegetation resistance to climate to different extents at the grid scale ( $R = 0.43 \pm 0.10$  for temperature,  $R = 0.28 \pm 0.12$  for precipitation, and  $R = 0.22 \pm 0.08$  for radiation); however, they are unable to capture patterns of vegetation resilience ( $R = 0.05 \pm 0.17$ ). Furthermore, vegetation resilience and resistance to climate change have regionally changed over the last three decades. In particular, the results suggest that vegetation resilience has increased in tropical forests and that vegetation resistance to temperature has increased in northern Eurasia. In contrast, ecosystem models cannot capture changes in vegetation resilience and resistance over the past thirty years. Overall, this study establishes a benchmark of vegetation resilience and resistance to climate change at the global scale, which is useful for further understanding ecological mechanisms of vegetation dynamics and improving ecosystem models, especially for dynamic resilience and resistance.

**Keywords:** resilience; resistance; climate change; remote sensing; vegetation growth; LAI



**Citation:** Sun, N.; Liu, N.; Zhao, X.; Zhao, J.; Wang, H.; Wu, D. Evaluation of Spatiotemporal Resilience and Resistance of Global Vegetation Responses to Climate Change. *Remote Sens.* **2022**, *14*, 4332. <https://doi.org/10.3390/rs14174332>

Academic Editor: Hirohiko Nagano

Received: 8 June 2022

Accepted: 29 August 2022

Published: 1 September 2022

**Publisher's Note:** MDPI stays neutral with regard to jurisdictional claims in published maps and institutional affiliations.



**Copyright:** © 2022 by the authors. Licensee MDPI, Basel, Switzerland. This article is an open access article distributed under the terms and conditions of the Creative Commons Attribution (CC BY) license (<https://creativecommons.org/licenses/by/4.0/>).

## 1. Introduction

Human-induced climate warming has exacerbated the instability of the climate system [1,2] and the climatic anomaly has significantly changed vegetation dynamics on a global scale, with significant impacts on ecosystem structure and function [3,4]. Changes in vegetation growth further affect the regional and global carbon and water cycles [5,6]. Thus, quantitative assessment of vegetation stability helps clarify the relationships between vegetation growth and climatic anomalies and understand changes in affected ecosystem functions [7,8] with significant ecological and economic implications.

Generally, two fundamental characteristics, resilience and resistance, are used to characterize vegetation stability in response to short-term climate anomalies [7,9–11]. Many studies have discussed vegetation resilience and resistance on regional and global scales

using different methods. For example, Indian terrestrial ecosystems are relatively fragile, and one-third of watersheds and most vegetation types are less resilient to drought [12]. Half of the catchments in Peninsular India are not hydrologically resilient to climatic warming shifts [13]. In the tropics and southwest China, more drought events make forests less resilient [14,15]. Higher daily minimum temperatures promote slower tree growth in tropical forests, which are less resilient to higher temperatures [15]. In terms of vegetation resistance, African tropical forests are resistant to extreme climate anomalies in 2015–2016 El Niño [16]. Observational evidence indicates that the temperature sensitivities of vegetation growth in boreal regions have been weakened in recent decades [17]. In addition, the maximum air temperature has exceeded the optimum air temperature for tropical forests [18], and the increasing temperature has negative effects on tropical forest growth [19]. All these findings strongly imply that vegetation stability in response to climate change might have changed during the last three decades, and such a change can be expected to affect the successional trajectory of global vegetation growth. However, this possibility has not yet been confirmed because the evidence for vegetation stability change on a global scale remains lacking.

With the advancement of sensors, datasets detected by remote sensing have long-term, continuous, and multi-scale features, providing information on a broad spatial range and being highly valuable for ecosystem research. Metrics characterizing ecosystem function and biomass and greenness of vegetation, including normalized difference vegetation index (NDVI) [11,20], enhanced vegetation index (EVI) [21], leaf area index (LAI) [22], vegetation optical depth (VOD) [21], and net primary productivity (NPP) [23], have advantages in quantifying vegetation responses to climate anomalies. For example, the linear slope of the deseasonalized NDVI was used as a proxy for vegetation resilience after drought [11,20]. Forest resilience was measured by a lag-1 autocorrelation coefficient of EVI anomaly or VOD anomaly [21]. Terrestrial ecosystem resilience was a ratio of the magnitude of maximum stress from which the LAI can recover to the length of time required for the LAI to recover to its normal range [22]. Some studies combined autoregressive models with NPP or EVI time series to extract resilience and resistance to assess vegetation stability [23,24]. Because of long-term and global coverage, these metrics provide a unique opportunity to assess the spatiotemporal resilience and resistance of global vegetation responses to climate change over the past three decades.

Regarding the status of vegetation stability research, there are three main deficiencies in work focused on responses of vegetation resilience and resistance to climate change. First, there are still few studies that comprehensively assess the resilience and resistance of vegetation to climate changes in variables such as temperature, precipitation, and radiation on a global scale. Second, although ecosystem models are widely used to simulate global vegetation dynamics, it is still not clear whether the models can capture observation-based vegetation resilience and resistance. Third, previous studies only considered the static patterns of vegetation stability [9,15,25] and did not assess the potentially dynamic patterns of vegetation resilience and resistance over the past decades.

Vegetation resilience is the rate at which vegetation recovers to its normal patterns during or after environmental perturbations, whereas vegetation resistance is the extent to which vegetation resists the changes in environmental factors [26]. In this study, we calculate vegetation resilience and resistance through autoregressive models [23,27]. Vegetation resilience can be characterized on the basis of long-term time series data from the relationships between ecosystem metrics in the current state and the previous state [10]. A larger magnitude of the regression coefficient between the current state and the previous state, which indicates stronger memory effects of vegetation, usually represents lower vegetation resilience, whereas a smaller magnitude typically indicates higher vegetation resilience. Resistance expresses the ability of vegetation to withstand environmental disturbances. Vegetation resistance is analogous to the sensitivity of vegetation to climate (e.g., temperature and precipitation), whereas the difference is that all the variables need

to be standardized in the autoregressive model [24,27], which can be used to compare the variation in vegetation growth in response to different climatic variables.

The primary objective of this study is to assess the spatial patterns and trends of observation- and model-based vegetation resilience and resistance on a global scale over the last three decades and to compare resilience and resistance in different biomes. There are two key problems that we are trying to solve. First, whether ecological models can capture observation-based spatial patterns and trends in vegetation resilience and resistance. Second, the unclear underlying dynamic patterns of vegetation resilience and resistance over the past few decades.

Because remote sensing scientists and ecosystem modelers both provide long-term LAI time series for 1982–2015 [28,29], it is a unique opportunity to evaluate the spatiotemporal resilience and resistance of global vegetation responses to climate change in the last three decades. Here, we first evaluated the applicability of LAI. In addition, we analyzed the global static spatial patterns of vegetation resilience and resistance (i.e., temperature, precipitation, and radiation) based on an autoregressive model. Then, we assessed whether the models can capture patterns of vegetation resilience and resistance on grid and biome scales. Finally, we examined the potential changes in vegetation resilience and resistance over the last three decades with a moving temporal window of fifteen years. Our statistical analyses and calculations are based on MATLAB R2020b software.

## 2. Materials and Methods

### 2.1. Remotely Sensed LAI Time Series

The Global Inventory Modeling and Mapping Studies (GIMMS) LAI 3g dataset of 1982–2015 was used to quantify the spatial patterns of vegetation resilience and resistance [22,28,30]. The spatial resolution of the GIMMS LAI was  $0.083^\circ \times 0.083^\circ$ , and the temporal resolution was 15 days. The semi-monthly GIMMS LAI time series were composited to monthly series using the maximum-value composition (MVC) method [31,32]. To match the spatial resolutions of the climate data and ecosystem models, GIMMS LAI datasets were resampled to a common spatial resolution of  $0.5^\circ \times 0.5^\circ$  with mean aggregation for all pixels. Pixels with multi-year averaged GIMMS LAI  $< 0.2$  were removed from the analyses, which mainly exclude areas with extremely sparse or non-existent vegetation cover [24].

### 2.2. Simulated LAI Time Series by Ecosystem Models

Although ecosystem models are widely used to simulate global vegetation dynamics, it is still not clear whether the models can capture observation-based vegetation resilience and resistance. To evaluate vegetation resilience and resistance, six state-of-the-art Trendy-v6 Dynamic Global Vegetation Models (DGVMs) were used in this study, including CABLE, ISAM, LPJ-GUESS, ORCHIDEE, VEGAS, and VISIT [29]. Among all ecological models of Trendy-v6 DGVMs, we first selected the model whose output simulated LAI. Second, only the six selected models' outputs simulated LAIs with  $0.5^\circ \times 0.5^\circ$  spatial resolution, which is consistent with the resolution used in the study. The simulated datasets were provided by the Global Carbon Project, which covers the historical period from 1982–2015. All the ecosystem models are forced by a set of observation-based time series data. In detail, atmospheric CO<sub>2</sub> concentration data is from the United States National Oceanic and Atmospheric Administration Earth System Research Laboratory (NOAA/ESRL) and Scripps Institution of Oceanography [29]; climate data is from the Climatic Research Unit and National Centers for Environmental Prediction Reanalysis products (CRU–NCEP v8) [33], and human-induced land use changes and management are from the History Database of the Global Environment (HYDE) and the Land-Use Harmonization v2 datasets [34,35]. The ecosystem output parameters from each model mainly include the vegetation index (LAI), carbon cycle data (carbon storage and carbon flux), nitrogen cycle data (nitrogen storage and nitrogen flux), and water cycle data (soil moisture, transpiration, and runoff). In this study, we mainly used monthly LAI time series based on the S3 simulation scenario (vary-

ing CO<sub>2</sub> concentrations over time, varying climate change over time, and varying land use changes over time) [36], which is considered a scenario similar to the real natural ecosystem.

### 2.3. Climatic Time Series

In our study, the monthly Climatic Research Unit gridded Time Series (CRU TS) V4 1982–2015 dataset with a spatial resolution of  $0.5^\circ \times 0.5^\circ$  was used to represent the climatic dynamics of the last three decades [37]. Few studies comprehensively evaluate the spatiotemporal resilience and resistance of global vegetation responses to climate change (i.e., temperature, precipitation, and radiation). To evaluate vegetation resistance to climate factors, three climatic variables—air temperature, precipitation, and solar shortwave radiation—were selected for interpreting vegetation resistance to climate. More importantly, the climate-forced data for all ecosystem models of Trendy-v6 DGVMs are the CRU dataset [33]. The CRU dataset was therefore chosen so that the same climate data can reduce climate errors in the analysis, allowing model-based vegetation resilience and resistance to better compare with observation-based results. The CRU dataset usually has good performance for climatic anomalies and is widely used in global change ecology research [38,39].

### 2.4. Biome Map

To analyze the vegetation resilience and resistance of different biome functional types, we created a biome map based on the Moderate Resolution Imaging Spectroradiometer (MODIS) Land Cover Climate Modeling Grid (CMG) Version 6 (MCD12C1 V6) dataset [40], widely used as a classification system in ecosystem studies [41–44]. The same vegetation type generally means that the hydrothermal environment of the ecosystem is roughly similar. The MODIS land cover dataset mainly contains three classification systems, the International Geosphere-Biosphere Programme (IGBP) system, the University of Maryland (UMD) system, and the leaf area index (LAI), which are provided at yearly intervals at  $0.05^\circ$ . In this study, we adopted the widely used IGBP classification system to make a biome map following specific synthetic rules [41]. We mainly focused on eight natural vegetation types, including tundra, boreal forest, tropical forest, temperate forest, shrubland, grassland, savanna, and woody savanna. The specific synthesis rules for the biome map are as follows:

- (1) Tundra: grassland and open shrubland north of  $55^\circ\text{N}$ ;
- (2) Boreal forest: evergreen needleleaf forest, deciduous needleleaf forest, and mixed forest north of  $50^\circ\text{N}$ ;
- (3) Tropical forest: evergreen broadleaf forest;
- (4) Temperate forest: deciduous broadleaf forest and mixed forest south of  $50^\circ\text{N}$ ;
- (5) Shrubland: open shrubland south of  $55^\circ\text{N}$ ;
- (6) Grassland: grassland south of  $55^\circ\text{N}$ ;
- (7) Savanna: same as savanna in the MODIS IGBP;
- (8) Woody savanna: same as woody savanna in the MODIS IGBP;

To minimize the influences of land use changes due to human activities, we constructed an unchanged land cover map for 2001 to 2015 (Figure S9) [42]. The unchanged biome map was further used to analyze vegetation resilience and resistance among different types.

### 2.5. Decomposition of the LAI and Climate Time Series

The time series of LAI and climatic variables with periodic changes are usually composed of three parts: long-term trend, intra-annual seasonality, and anomaly. Accordingly, the periodic time series can be written as follows:

$$Y = \text{Trend} + \text{Seasonality} + \text{Anomaly} \quad (1)$$

where  $Y$  is the monthly LAI or climate time series, Trend is the long-term trend, Seasonality is the seasonal cycle, and Anomaly denotes the anomalies compared to normal conditions [45].

In this study, vegetational and climatic anomalies were applied to quantify vegetation resilience and resistance. First, we removed the seasonality of vegetational and climatic time series via a multiyear averaged seasonal cycle. Second, we obtained the anomalies after detrending the time series via a linear regression model using the regress function in MATLAB. Third, we normalized the time series of anomalies using the Z-score normalization method to calculate vegetation resilience and resistance.

### 2.6. Vegetation Resilience and Resistance

We used a multiple linear regression model to quantify vegetation resilience and resistance using the fitlm function in MATLAB. Here, the time series of the LAI anomaly was treated as the dependent variable, and the time series of the LAI anomaly with a one-month lag and the time series of the climate anomalies, including temperature, precipitation, and solar radiation anomalies, were treated as the independent variables. The expression of the autoregressive model can be written as follows:

$$LAI_t = \alpha * LAI_{t-1} + \beta * T_t + \gamma * P_t + \delta * R_t + \epsilon_t \quad (2)$$

Here,  $LAI_t$  is the time series of the normalized LAI anomaly;  $LAI_{t-1}$  is the time series of the normalized LAI anomaly with a one-month lag;  $T$ ,  $P$ , and  $R$  represent the time series of temperature, precipitation, and radiation anomalies, respectively;  $\epsilon_t$  is the residual term.  $\alpha$ ,  $\beta$ ,  $\gamma$ , and  $\delta$  are the model coefficients, which range from  $-1$  to  $1$ . Specifically,  $\alpha$  represents vegetation resilience and  $\beta$ ,  $\gamma$ , and  $\delta$  represent vegetation resistance to temperature, precipitation, and solar radiation, respectively. Here, larger absolute values of vegetation resilience and resistance indicate lower resilience and lower resistance, and vice versa. Positive  $\beta$ ,  $\gamma$ , or  $\delta$  values indicate that higher temperature, more precipitation, or stronger radiation can promote vegetation growth. Negative  $\beta$ ,  $\gamma$ , or  $\delta$  values indicate that higher temperatures, more precipitation, or stronger radiation can inhibit vegetation growth. The significance of vegetation resilience or resistance is tested at the level of  $p < 0.05$ .

### 2.7. The Temporal Changes in Vegetation Resilience and Resistance

The temporal changes in vegetation resilience and resistance were analyzed by using a 15 years moving temporal window algorithm from 1982 to 2015. The starting year of the first temporal window of vegetation resilience and resistance was 1982 and the ending year was 1996. The temporal window slid by 1 year for each step, with the last temporal window being 2001–2015. Then, we calculated linear trends of vegetation resilience and resistance using the regress function in MATLAB through 20 temporal windows on a pixel scale. Here, the significance of the change in vegetation resilience or resistance is tested at the level of  $p < 0.05$ . Finally, the trends were compared between observed and modeled resilience and resistance within different biomes. We tested the uncertainty analyses of the autoregression model using different window sizes including 10 years, 15 years, and 20 years. We plot the spatial patterns and frequency distribution of the changes in observation-based vegetation resilience and resistance among the three window sizes. Results are consistent among different window sizes, which verified the robustness of the conclusions in terms of changes in vegetation resilience and resistance (Figures S10 and S11).

## 3. Results

### 3.1. Applicability of LAI

To evaluate the applicability of the model-simulated LAI, we also compared the LAI based on remote sensing observations and model simulation. The results show that the LAI in six models is roughly similar to the spatial gradient of the GIMMS LAI (Figure S1). The correlation between GIMMS LAI and six DGVMs LAI is relatively high, with  $R$  ranging from 0.57 for VISIT to 0.90 for ISAM (Figure 1). To evaluate the results based on GIMMS LAI, we further calculated vegetation resilience and resistance to climate variables based on GIMMS NDVI (Figure S2). The spatial pattern and relative magnitude of vegetation resilience and resistance based on GIMMS NDVI are consistent with the results based

on GIMMS LAI (Figures 2 and S2). Therefore, choosing LAI as a vegetation feature can accurately reflect vegetation resilience and resistance.

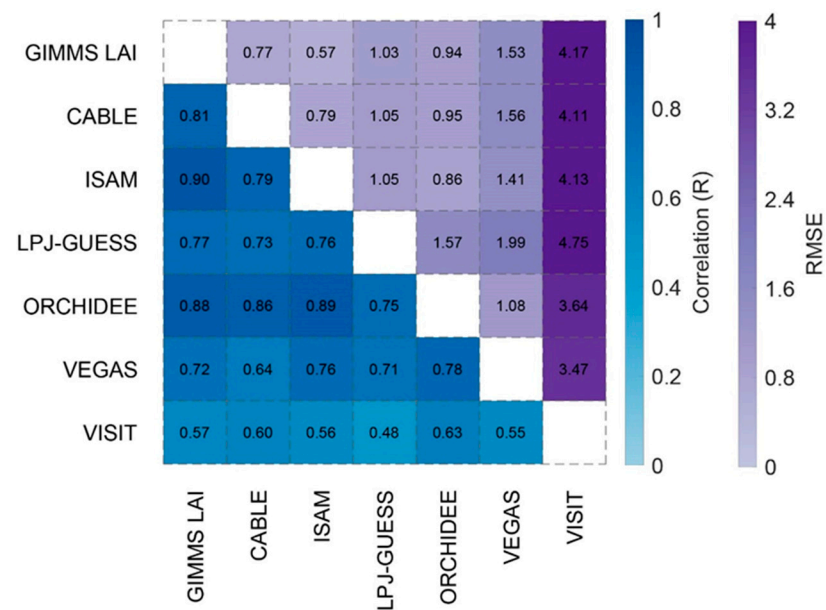


**Figure 1.** Pearson correlation and root-mean-square error (RMSE) between annually averaged GIMMS LAI and modeled LAI from 1982 to 2015 at the grid scale.

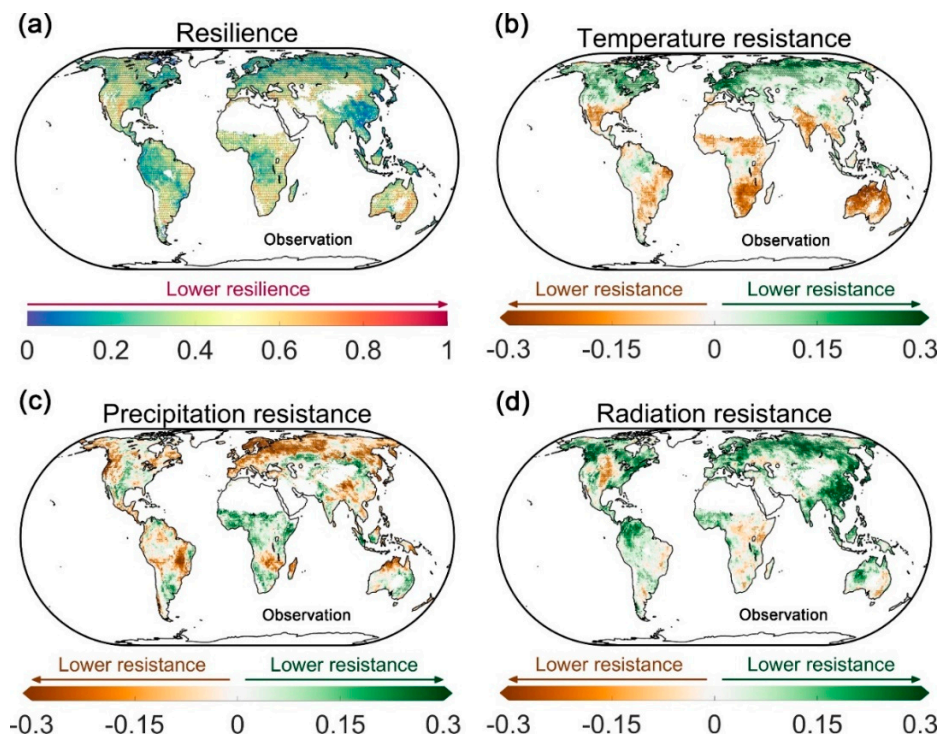


**Figure 2.** Spatial patterns of vegetation resilience and resistance to climatic variables based on GIMMS LAI: (a) vegetation resilience; (b) temperature resistance; (c) precipitation resistance; (d) radiation resistance. In each subfigure, stippling indicates that the vegetation resilience or climatic resistance is significant ( $p < 0.05$ ) in the grid. Vegetation resilience is within the range of 0 and 1, and larger values suggest lower resilience. Climatic resistance is within the range of  $-1$  and  $1$ , and values with larger absolute magnitudes indicate lower climatic resistance.

### 3.2. Spatial Patterns of Vegetation Resilience and Resistance

Based on the autoregressive model, the vegetation resilience and resistance reveal clear spatial patterns (Figure 2a). Stronger vegetation resilience is observed in northern Eurasia, eastern North America, the Amazon Basin, central Africa, and southeastern Asia. The results suggest that the rate at which an ecosystem recovers to its normal patterns during or after environmental perturbations is faster in these regions. In contrast, vegetation resilience in arid and semiarid regions is generally lower, which indicates that vegetation in these regions takes longer to recover to its original state during or after environmental disturbances.

Vegetation resistance to temperature is negative in South Asia and arid and semiarid regions such as Mexico, southern South America, Sub-Saharan Africa, southern Africa, and Australia (Figure 2b). This means that vegetation growth can be limited if the regional temperature increases. Furthermore, the resistance of vegetation to temperature anomalies is lower in arid and semiarid regions (e.g., Australia, Sub-Saharan Africa, and southern Africa). In addition, vegetation resistance to temperature anomalies in the high northern latitudes is positive, indicating that increasing temperature in these regions can promote local vegetation growth.

Vegetation resistance to precipitation and resistance to temperature generally show opposite effects (Figure 2b,c). For example, at high northern latitudes, vegetation growth is negatively related to precipitation anomalies; however, the relationship is positive for arid and semiarid regions (Figure 2c). These results indicate that a short-term increase in precipitation will enhance vegetation growth more in water-limited regions, whereas it will weaken vegetation growth to a greater extent in temperature-limited regions.

Vegetation resistance to radiation anomalies is positive in most regions of the world (Figure 2d), indicating that stronger radiation usually promotes vegetation growth. Meanwhile, in high northern latitudes, southeastern Asia, the northern Amazon, and western Australia, vegetation is less resistant to radiation anomalies, which means that a short-term increase in radiation will enhance vegetation growth to a greater extent. For parts of North-western America, the main limiting factor of vegetation growth is water (Figure 2d), and more radiation (also higher temperature) in water-limited regions might restrict vegetation growth [24]. In other regions of the world, such as arid and semiarid regions, vegetation resistance to radiation is stronger, which means that vegetation growth is less sensitive to radiation in these regions.

Averaged vegetation resilience from the six Trendy-v6 DGVMs does not capture the spatial patterns of vegetation resilience by observations (Figures 2a and 3a). In comparison, the magnitudes of model-based vegetation resilience are much lower than the observation-based results. Specifically, vegetation resilience is lower in tropical regions according to the models; however, it is higher in tropical regions according to the observations. In addition, ecosystem models effectively capture the spatial patterns of vegetation resistance to temperature globally (Figures 2b and 3b), which suggests positive relations in temperate and boreal regions in the Northern Hemisphere. In addition, for vegetation resistance to precipitation, the models capture the positive relations in arid and semiarid regions (Figures 2c and 3c), whereas they do not effectively capture the negative relations in boreal regions. For vegetation resistance to radiation, averaged values of ecosystem models generally suggest weak relations (Figures 2d and 3d), which means radiation is less important than temperature and precipitation for vegetation growth in models. However, the observation-based results tell another story about the resistance of vegetation to radiation.

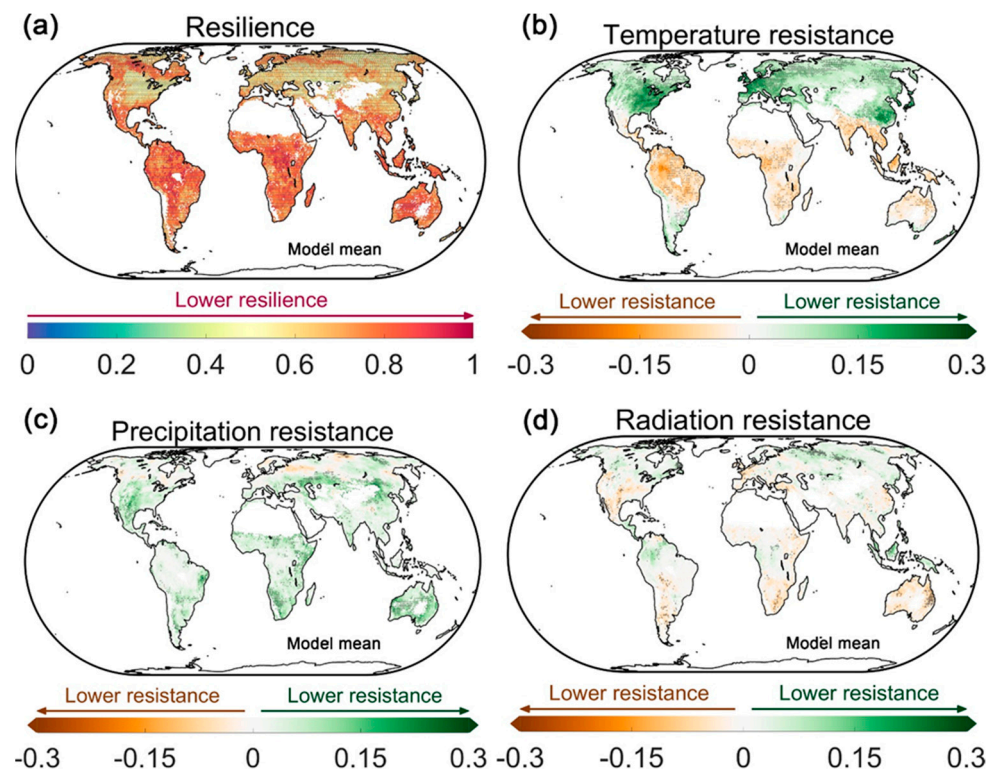


**Figure 3.** Spatial patterns of averaged vegetation resilience and resistance to climatic variables by six DGVMs: (a) vegetation resilience; (b) temperature resistance; (c) precipitation resistance; (d) radiation resistance. If the vegetation resilience or climate resistance are significant ( $p < 0.05$ ) in more than 3 models in a pixel, averaged vegetation resilience and resistance to climatic variables by six DGVMs are significant in that pixel. In each subfigure, stippling indicates that the vegetation resilience or climatic resistance is significant ( $p < 0.05$ ). Vegetation resilience is within the range of 0 and 1, and larger values suggest lower resilience. Climatic resistance is within the range of  $-1$  and  $1$ , and values with larger absolute magnitudes indicate lower climatic resistance.

### 3.3. Evaluation of Modeled Vegetation Resilience and Resistance

To quantify how well ecosystem models capture the spatial patterns of vegetation resilience and resistance, we first calculated the Pearson correlation and RMSE between observation- and model-based results on a grid scale. The results suggest that most of the models do not capture the observation-based vegetation resilience, with  $R$  ranging from  $-0.29$  for LPJ-GUESS to  $0.28$  for ORCHIDEE and RMSE ranging from  $0.35$  for ISAM to  $0.51$  for VISIT (Figure 4a). In contrast, most of the models capture the patterns of vegetation resistance to temperature well, with  $R$  ranging from  $0.29$  for VISIT to  $0.58$  for ORCHIDEE and RMSE ranging from  $0.11$  for ORCHIDEE to  $0.17$  for VISIT (Figure 4b). Compared to vegetation resistance to temperature, the models do not effectively capture vegetation resistance to precipitation ( $R$  values range from  $0.15$  for VISIT to  $0.49$  for LPJ-GUESS) and radiation ( $R$  values range from  $0.08$  for ISAM to  $0.33$  for ORCHIDEE) (Figure 4c,d). Specifically, among the six ecosystem models, ORCHIDEE showed the best performance when comparing observation-based vegetation resilience and resistance.

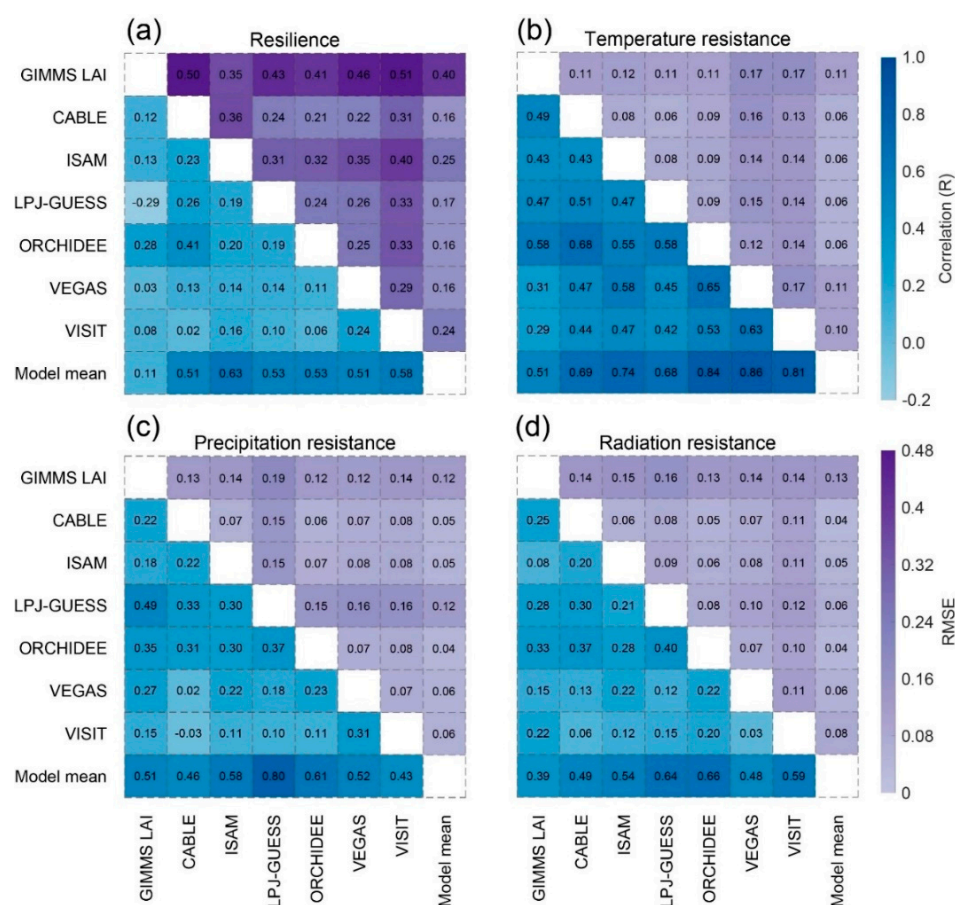


**Figure 4.** Pearson correlation and root-mean-square error (RMSE) between observation- and model-based vegetation resilience and resistance at the grid scale: (a) vegetation resilience; (b) temperature resistance; (c) precipitation resistance; (d) radiation resistance.

In addition to spatial patterns, we also evaluated the modeled vegetation resilience and resistance at the biome scale. Observation-based results suggest that the resilience of water-limited shrubland and grassland is weak. Excessive temperatures have negative effects on shrubland. Tundra and boreal forest in high altitudes are not bound by precipitation. Radiation enhancement promotes the growth of all types of vegetation (Figure 5). For observation-based results, the median value of vegetation resilience in the tundra, boreal forest, tropical forest, temperate forest, savanna, and woody savanna areas ranged from 0.2407 to 0.3054, and the values for water-limited shrubland and grassland were 0.5053 and 0.4662, respectively (Figure 5a and Table S1). In comparison, median values of modeled vegetation resilience across the eight natural biomes range from 0.5945 to 0.7984, far exceeding the observation-based results. The large difference indicates that the vegetation recovery rate after climatic disturbance in ecosystem models is much slower than that in the real ecosystem. In addition, the modeled vegetation resistance to temperature is quite similar to the observation-based results (the mean value is 0.0395 for observations and 0.0407 for model means) (Figure 5b and Table S1), which indicates that the ecosystem model is more reliable in capturing vegetation–temperature interactions. For vegetation resistance to precipitation, the sign of the modeled results is the opposite of that of the observed results for tundra (−0.0676 versus 0.0125), tropical forest (−0.0186 versus 0.0188), temperate forest (−0.0697 versus 0.0266), savanna (−0.0451 versus 0.0344), and woody savanna areas (−0.0709 versus 0.0233), whereas the models only capture vegetation–precipitation interactions well for shrubland (0.0303 versus 0.0957) and grassland (0.0493 versus 0.0744) (Figure 5c and Table S1). For vegetation resistance to radiation, the observed values for the biomes ranged from 0.0226 for grassland to 0.2002 for temperate forest; however,

the modeled results were all approximately zero (ranging from  $-0.0332$  for shrubland to  $0.0345$  for boreal forest) (Figure 5d and Table S1), which means that vegetation–radiation interactions were poorly evaluated in most ecosystem models.

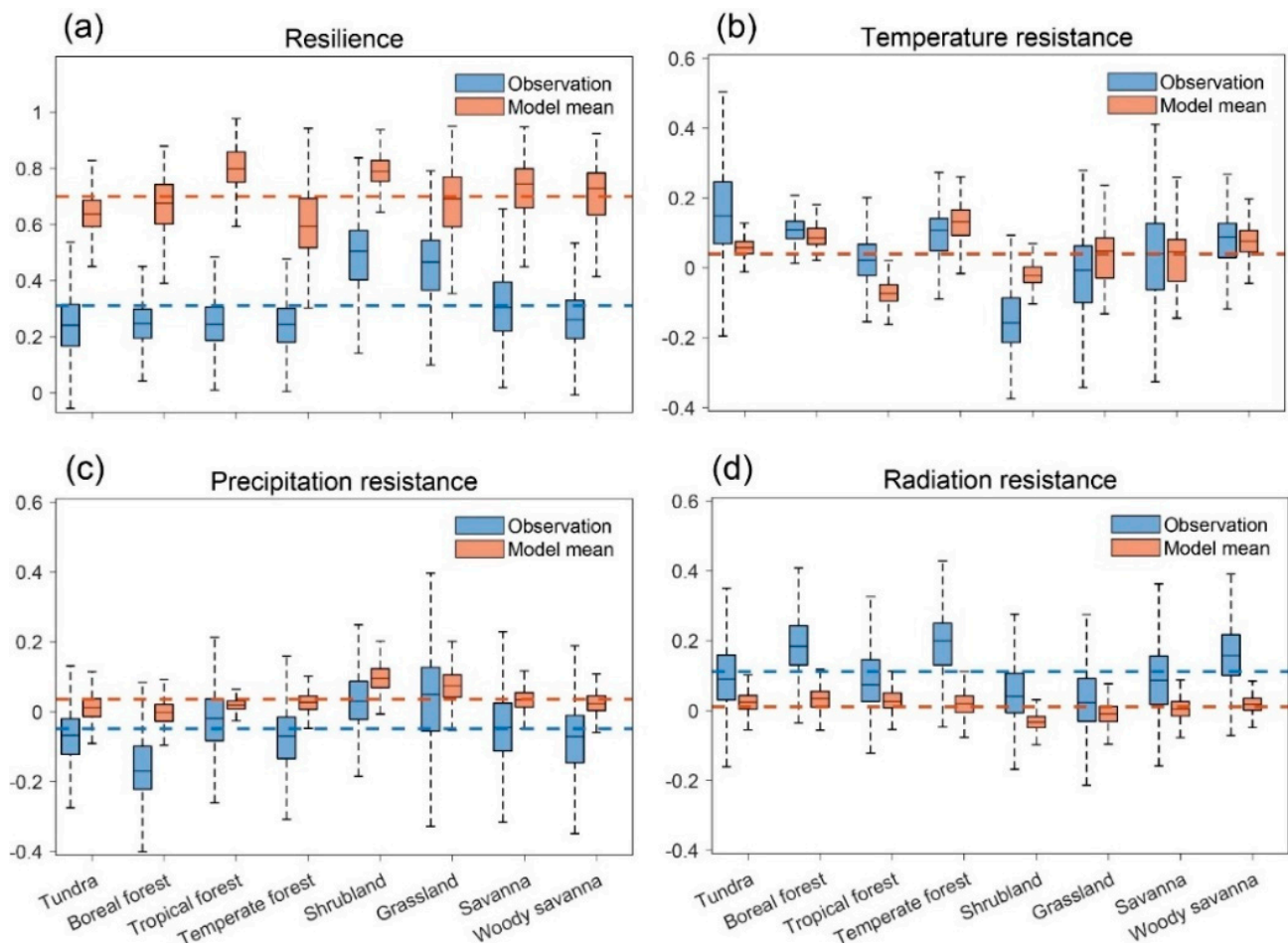


**Figure 5.** Box plot of observation and model mean vegetation resilience and resistance at the biome scale: (a) vegetation resilience; (b) temperature resistance; (c) precipitation resistance; (d) radiation resistance. The horizontal dashed lines represent the mean vegetation resilience and resistance of the eight biomes.

Given that the correlation between modeled and observed resilience and resistance may be the high criterion, we also established linear relations between the two at the biome scale. In general, the conclusions are similar to those made at the grid scale. In other words, the ecosystem models did not capture the observed vegetation resilience well ( $R^2$  ranged from 0.00 for CABLE to 0.41 for ISAM) (Figure 6a). In addition, vegetation resistance to temperature ( $R^2$  ranged from 0.03 for VISIT to 0.78 for CABLE) and to precipitation ( $R^2$  ranged from 0.34 for ISAM to 0.80 for VEGAS) suggest a more robust relationship between the model and observations, followed by vegetation resistance to radiation ( $R^2$  ranged from 0.02 for VISIT to 0.63 for VEGAS) (Figure 6b–d). Even though there is a good relationship between the observations and models for vegetation resistance, the magnitudes still show a considerable bias from the 1:1 line, which should be further studied with ecosystem modelers. Among the ecosystem models, VEGAS shows better performance in capturing vegetation resilience ( $R^2 = 0.37$ ) and resistance ( $R^2 = 0.25$  for temperature,  $R^2 = 0.80$  for precipitation,  $R^2 = 0.63$  for radiation) at the biome scale.

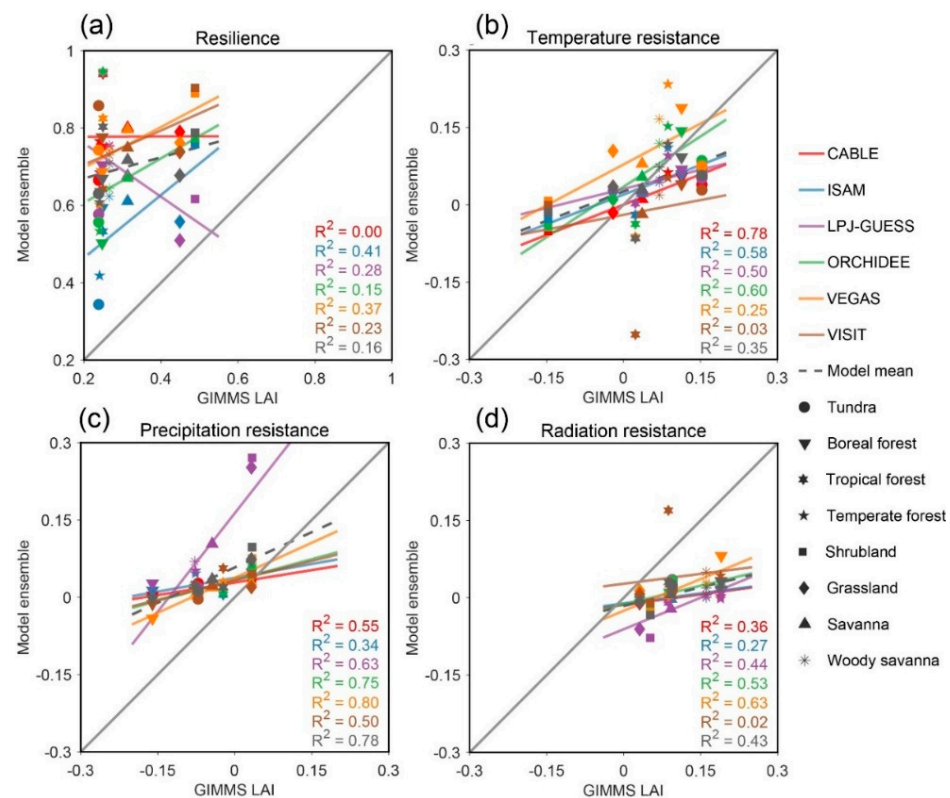


**Figure 6.** Linear relationship between observation- and model-based vegetation resilience and resistance at the biome scale: (a) vegetation resilience; (b) temperature resistance; (c) precipitation resistance; (d) radiation resistance. Different colors represent the six ecosystem models, and different shapes represent the eight biomes. The colored lines represent fitted regression lines.

### 3.4. Changes in Vegetation Resilience and Resistance

The dynamics of vegetation resilience and resistance are calculated with a moving window of 15 years from 1982 to 2015, and linear trends of vegetation resilience and resistance are derived on a pixel scale. Interestingly, the results suggest that vegetation resilience increased in most tropical forest (Figure 7a), which indicates that rates of vegetation recovery may be strengthened during or after environmental perturbations. Changes in vegetation resilience in other regions are irregular and fragmented. In comparison, the ecosystem model does not capture the increased resilience in tropical regions (Figure 7b). The results suggest that vegetation resistance to temperature increased in northeast Eurasia but decreased in India, Australia, and the Amazon Basin (Figure 7c). In other words, vegetation growth is no longer sensitive to temperature anomalies in northern Eurasia, whereas it is more sensitive to temperature changes in India, Australia, and the Amazon Basin. In comparison, the ecosystem model does not capture the changes in temperature resistance in these regions well (Figure 7d). The observed vegetation resistance to precipitation increased in western Eurasia, whereas the modeled results showed marginal changes (Figure 7e,f). Patterns of observed vegetation resistance to radiation are irregular and fragmented (Figure 7g,h).

To further quantitatively evaluate the changes in vegetation resilience and resistance, probability distributions of the changes were analyzed for the eight natural biomes. In general, the trend values of vegetation resilience and resistance calculated from the observations suggest a wide range, whereas trend values from models are narrowly distributed (Figure 8 and Table S2). This phenomenon indicates that vegetation in reality is more complex and driven by multiple ecological processes. However, ecosystem models usually consider some of the basic processes; therefore, the probability distribution is much narrower. Specifically, vegetation resilience is obviously increased in tropical forest (mean =  $-0.00994 \text{ year}^{-1}$ ),

whereas it is decreased in shrubland (mean = 0.00416 year<sup>-1</sup>). Vegetation resistance to temperature increased in tundra (mean = -0.00193 year<sup>-1</sup>), whereas it decreased in tropical forest (mean = 0.00229 year<sup>-1</sup>), temperate forest (mean = 0.00220 year<sup>-1</sup>) and shrubland (mean = 0.00229 year<sup>-1</sup>). Vegetation resistance to precipitation increased in tundra (mean = -0.00178 year<sup>-1</sup>) and boreal forest (mean = -0.00540 year<sup>-1</sup>), whereas it decreased in tropical forest (mean = 0.00227 year<sup>-1</sup>) and temperate forest (mean = 0.00251 year<sup>-1</sup>). Vegetation resistance to radiation decreased in tropical forest (mean = 0.00389 year<sup>-1</sup>) and shrubland (mean = 0.00343 year<sup>-1</sup>). Here, it should be noted that although we diagnosed changes in vegetation resistance to climate, the magnitudes of the mean values are relatively small because of wide distribution ranges driven by complex processes under actual conditions. However, none of the ecosystem models capture the changes in vegetation resilience and resistance, with mean values of approximately zero (ranging from -0.00524 year<sup>-1</sup> for tundra resilience in ISAM to 0.00378 year<sup>-1</sup> for shrubland radiation resistance in LPJ-GUESS).

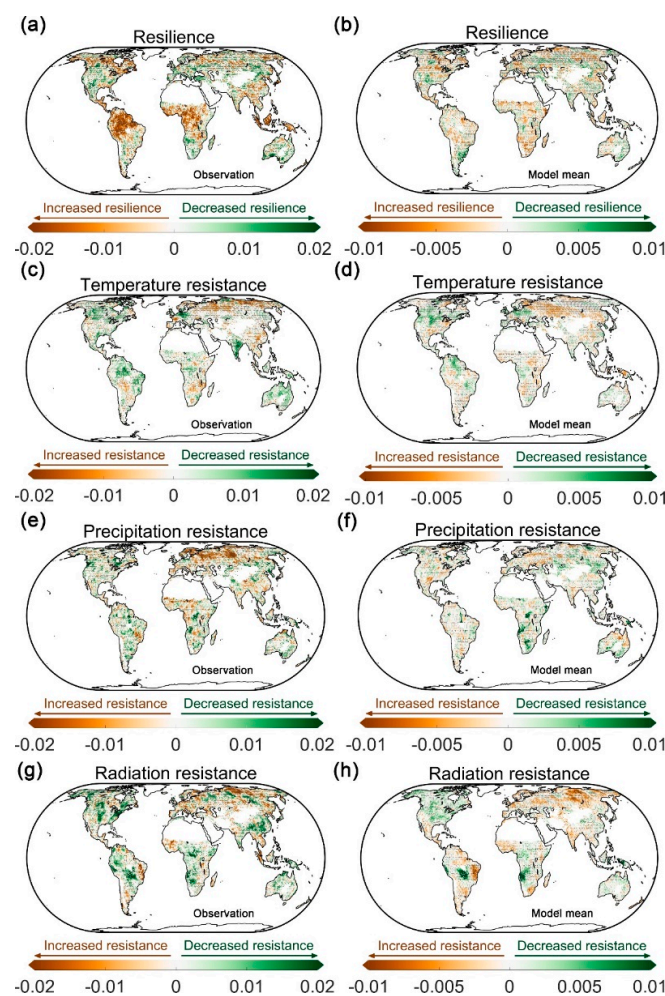


**Figure 7.** Spatial patterns of the changes in vegetation resilience and resistance derived from observations and models from 1982 to 2015: The changes in observation-based (a) vegetation resilience; (c) temperature resistance; (e) precipitation resistance; (g) radiation resistance. The changes in (b) vegetation resilience; (d) temperature resistance; (f) precipitation resistance; (h) radiation resistance. Linear trends of vegetation resilience and resistance are derived with sliding windows of 15 years step. If the changes in vegetation resilience or climatic resistance are significant ( $p < 0.05$ ) in more than 3 models, the change in model-based vegetation resilience or climatic resistance is significant ( $p < 0.05$ ). In each subfigure, stippling indicates that the changes in observation-based and model-based vegetation resilience or climatic resistance are significant ( $p < 0.05$ ) in the grid. A positive value of the linear trend represents decreased resilience and resistance, and a negative value of the linear trend represents increased resilience and resistance.

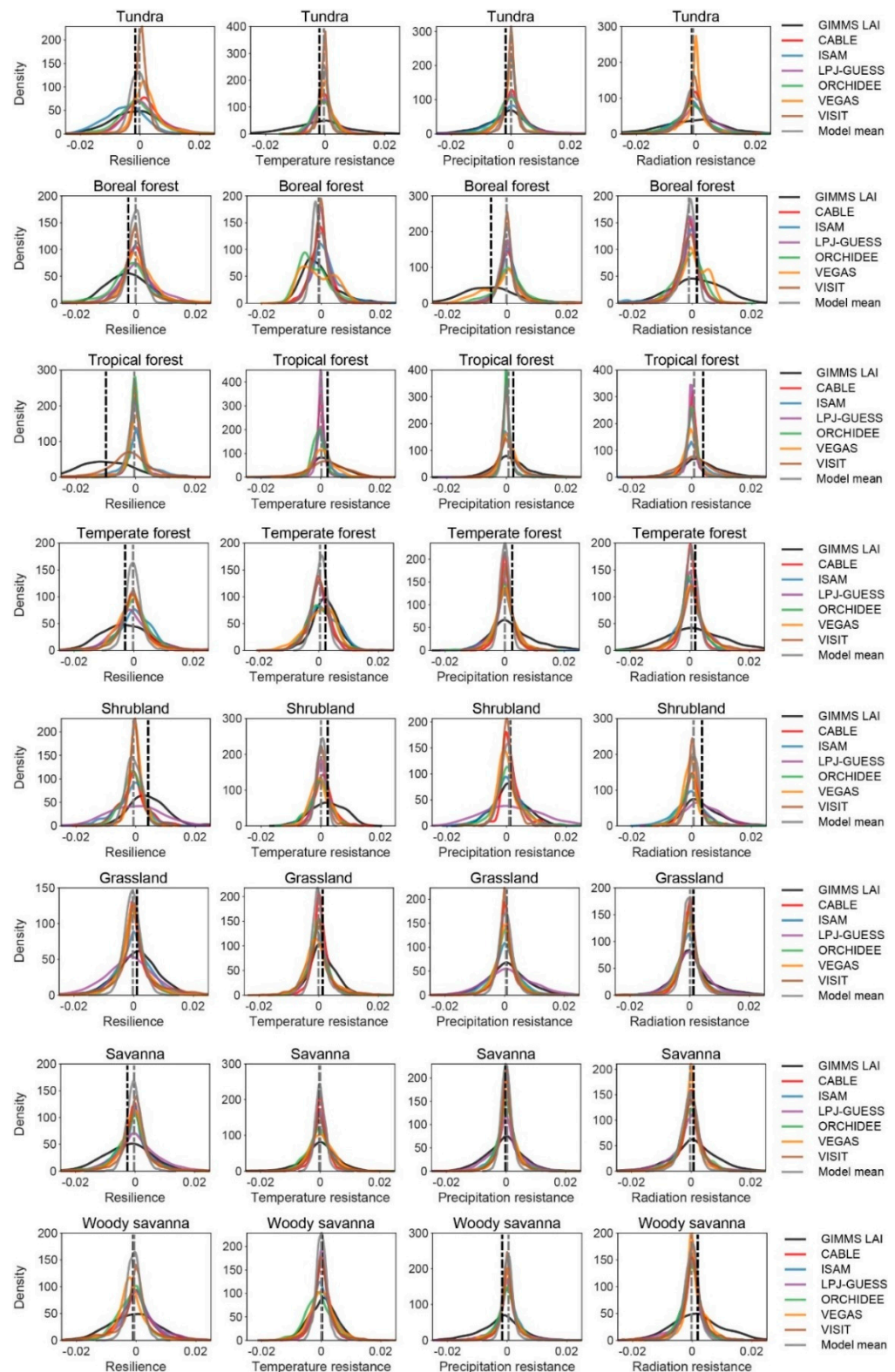


**Figure 8.** Probability distributions of the changes in vegetation resilience and resistance derived from observations and models at the biome scale. The eight biomes include tundra, boreal forest, tropical forest, temperate forest, shrubland, grassland, savanna, and woody savanna. The gray dashed line represents the mean vegetation resilience and resistance of the GIMMS LAI. The black dashed line represents the mean vegetation resilience and resistance changes of the model mean. The distribution curves are fitted with kernel smoothing function estimates for vegetation resilience and resistance changes.

## 4. Discussion

### 4.1. Driving Mechanisms of Vegetation Resilience and Resistance

The spatial patterns of vegetation resilience demonstrated in our study are similar to those reported in related studies [25,27,46]. In arid and semiarid regions (e.g., the west of the United States, Sub-Saharan Africa, and Australia), low resilience suggests strong self-memory of vegetation growth, which means that vegetation recovers slowly to its normal state during or after climatic disturbances. Furthermore, due to low resilience, vegetation such as savanna can easily transition into an alternative state in response to climate change [47]. For example, increased annual precipitation over long periods in Sub-Saharan Africa may promote a shift in vegetation from savanna to woody savanna or forest, whereas increased water stress may promote a shift from savanna to grassland or desert [47]. In contrast, the high resilience in tropical forest implies that recovery rates following environmental disturbance are high [15,48]. The biome resilience decreased when the vegetation becomes barren or sparse [23]. Tropical forest with high species diversity is more complex in composition and structure than other vegetation systems. Therefore, tropical forest is much more resilient than other biomes [22,49]. For example, the ecosystem stability of the study area decreased from forest to cropland, shrub, and barren grassland [23]. Although tropical forest is much more resilient than other biomes, the significant dependence of vegetation resilience on precipitation suggests that the vegetation state may change in response to future climate change [47].

The climatic resistance of vegetation observed in our study suggests clear patterns. Compared with previous studies [24,42,50], our study reveals similar patterns of temperature, precipitation, and radiation resistance. For example, vegetation at high northern latitudes shows less temperature resistance; vegetation in arid and semiarid regions shows less precipitation resistance, and tropical forest shows less radiation resistance [24]. In other words, the underlying ecological mechanisms are closely related to the basic local environment. At high northern latitudes, the temperature is a limiting factor for vegetation photosynthesis and there are two possible mechanisms behind the negative relationship between vegetation growth and precipitation anomalies. First, more precipitation at the high northern latitudes resulted in an increase in cloud cover and a further decrease in temperature. In these temperature-controlled regions, the decreased temperature may play negative effects on vegetation growth [38]. Second, soil moisture is high at the high northern latitudes, so vegetation growth is not limited by precipitation. More precipitation may have negative effects on vegetation growth [36]. However, water is a limiting factor for vegetation growth in arid and semiarid regions. In addition, although climate conditions are close to optimal in tropical forests for vegetation growth, vegetation in high-density forests competes for light resources. This is why vegetation resistance to radiation is low in tropical forests. In previous studies, the patterns of the dominant climatic drivers in tropical forests were found to be irregular and fragmented [42], which may be the result of neglecting vegetation resilience in their multiple linear models. In contrast, the patterns based on the autoregression model found in our study produce clearer trends of vegetation resistance to different climatic factors.

Upon comparing the observation-based and model-based vegetation resilience results, we find that all ecosystem models do not capture the spatial gradients and that they do not even capture the relative magnitudes of vegetation resilience among natural biomes. This indicates that the processes related to resilience are still lacking in current models [51]. For example, different biomes usually have different recovery rates in response to climatic disturbance [25,52]. Usually, vegetation recovery after disturbance in natural experiments takes a long time [53,54], so the ground truth is very limited in interpreting the processes of vegetation resilience [55]. In contrast, most models can effectively capture vegetation resistance to temperature precipitation at the grid and biome scales. In the last three decades, interactions between temperature/precipitation and vegetation have been widely studied using field experiments and remote sensing [56,57]. Observation-based vegetation resilience is low in arid and semiarid regions [22]. The comparison shows that the model-

based vegetation resilience is lower in parts of arid and semi-arid regions, such as Sub-Saharan Africa and Australia (Figures 2a and 3a). However, some models, such as ISAM and LPJ-GUESS, failed to capture relatively low resilience in the arid and semiarid regions of Eurasia (Figures S4a and S5a). In the real world, vegetation in arid regions usually recovers slowly after disturbance. However, some models do not consider this process. The realistic findings obtained also help couple new processes and improve the parameterizations of ecosystem models. Therefore, our results in terms of vegetation resilience and resistance not only point out the weaknesses of current ecosystem models but are also useful for further understanding the ecological mechanisms of vegetation dynamics and improving ecosystem models.

#### 4.2. Implications of Changes in Vegetation Resilience and Resistance

The observed changes in vegetation resilience and resistance from 1982 to 2015 indicate that vegetation resilience and resistance dynamically respond to climate change. The results obtained from remotely sensed time series suggest that vegetation resilience in tropical forests increased in the later period, which suggests that vegetation may recover from environmental disturbance much faster. Such signals may also imply that the adaptation of tropical forests to climate change has increased [24]. In addition, temperature resistance has increased in northern Eurasia, which means that the sensitivity of vegetation to temperature has decreased. This phenomenon was also observed in a previous study in which the relationship between interannual variability in temperature and vegetation activity was found to have weakened [17]. The mechanisms may involve declining global warming effects on spring leaf unfolding and spring photosynthetic capacity [58]. Furthermore, our study demonstrates that precipitation resistance and radiation resistance also slightly increased, which implies that the vegetation at high northern latitudes cannot continue to respond at a pace with climate change.

Widely observed global vegetation dynamics are driven by many factors, including changes in vegetation resilience and resistance, climate change, nutrient fertilization, and land use change. Although multiple studies based on ecosystem models have attempted to explain global greening in the last three decades [59–62], few have considered the driving processes involved in terms of dynamic vegetation resilience and resistance in the last three decades. Because vegetation resilience and resistance are dynamic according to our results, our study raises a new scientific question. However, dynamic vegetation stability is still ignored in current ecosystem models because climatic sensitivities in these models are usually assumed to be constant parameters, and the processes related to the evolutionary response of vegetation to climate change remain unclear [63]. In future studies, dynamic vegetation stability processes should be considered in ecosystem models so that we can further diagnose the specific contributions of global vegetation dynamics.

#### 4.3. Uncertainty and Future Work

Based on the evaluation of spatiotemporal resilience and resistance of global vegetation responses to climate change conducted in our study, some remaining uncertainties should be further studied in the future to understand vegetation stability. First, in the autoregression linear regression model, the magnitude of vegetation resilience derived from remotely sensed time series shows obvious differences with ecosystem models. The biases may also relate to the signal-to-noise ratio in the time series of the LAI anomalies. Second, dynamic vegetation resilience and resistance may affect the successional trajectory of global vegetation growth in response to climate change. For example, temperature resistance has increased in northern Eurasia, which means that the sensitivity of vegetation to temperature has decreased and implies that the vegetation greening at high northern latitudes may not continue to quickly respond to pace with global warming. However, current ecosystem models do not capture dynamic vegetation resilience and resistance. Thus, we cannot quantify the relationship between vegetation resilience and resistance and global greening using prior models in the current time. To quantify the specific contributions

of environmental factors (i.e., dynamic CO<sub>2</sub> concentration, climate, land use change) and ecological factors (i.e., dynamic resilience and resistance), more comprehensive ecosystem models are required after considering dynamic vegetation stability. Third, other long-time series observations such as flux-net site observations should be used to further confirm the spatial patterns and temporal changes of vegetation resilience and resistance to climate.

## 5. Conclusions

In conclusion, our study comprehensively evaluated spatiotemporal vegetation resilience and resistance on different spatial scales using observations and models. LAI as a vegetation feature can accurately reflect vegetation resilience and resistance. Our results indicate that the autoregression model involving lag-1 vegetation anomalies can better describe vegetation resistance to different climatic factors. The results revealed clear spatial patterns of observation-based vegetation resilience and resistance over the last three decades. Observation-based vegetation resilience suggests clear spatial gradients; however, all ecosystem models are unable to capture the patterns of vegetation resilience. In contrast, ecosystem models can capture the resistance of vegetation to climatic factors to different extents (temperature > precipitation > radiation). In addition, based on observations, we observed regional changes in vegetation resilience and resistance for the last three decades; however, the changes from most models were irregular and fragmented. In summary, our study provides a benchmark of global vegetation stability that can be used to improve the ecosystem processes illustrated in ecosystem models. A well-developed ecosystem model considering dynamic vegetation stability is necessary to deeply understand the driving mechanisms of vegetation dynamics under rapid climate change.

**Supplementary Materials:** The following supporting information can be downloaded at: <https://www.mdpi.com/article/10.3390/rs14174332/s1>, Figure S1: spatial patterns of annually averaged GIMMS LAI and modeled LAI from 1982 to 2015; Figure S2: spatial patterns of averaged vegetation resilience and resistance to climatic variables based on GIMMS NDVI; Figure S3: spatial patterns of averaged vegetation resilience and resistance to climatic variables by CABLE; Figure S4: spatial patterns of averaged vegetation resilience and resistance to climatic variables by ISAM; Figure S5: spatial patterns of averaged vegetation resilience and resistance to climatic variables by LPJ-GUESS; Figure S6: spatial patterns of averaged vegetation resilience and resistance to climatic variables by ORCHIDEE; Figure S7: spatial patterns of averaged vegetation resilience and resistance to climatic variables by VEGAS; Figure S8: spatial patterns of averaged vegetation resilience and resistance to climatic variables by VISIT; Figure S9: biome map based on the MODIS IGBP system. The eight biomes include tundra, boreal forest, tropical forest, temperate forest, shrubland, grassland, savanna, and woody savanna; Figure S10: spatial patterns of the changes in observation-based vegetation resilience and resistance with different window sizes of 10 years, 15 years, and 20 years; Figure S11: probability distributions of the changes in observation-based vegetation resilience and resistance with different window sizes of 10 years, 15 years, and 20 years; Table S1: median values of observation and model mean vegetation resilience and resistance in eight natural biomes; Table S2: mean K values of vegetation resilience and resistance changes in eight natural biomes derived from observation and models.

**Author Contributions:** Conceptualization, X.Z. and D.W.; methodology, N.S. and D.W.; software, N.S. and N.L.; validation, N.S. and N.L.; formal analysis, N.S.; writing—original draft, N.S.; writing—review and editing, N.L., J.Z. and H.W. All authors have read and agreed to the published version of the manuscript.

**Funding:** This research was funded by the National Natural Science Foundation of China (42090012), the National Key Research and Development Program of China (No. 2016YFB0501404 and No. 2016YFA0600103), and the Natural Science Foundation of Anhui province of China (2008085QD167).

**Data Availability Statement:** Trendy-v6 DGVMs LAI is available at <https://sites.exeter.ac.uk/trendy/>, accessed on 22 September 2021. CRU TS V4 dataset is available at <http://www.cru.uea.ac.uk/data/>, accessed on 22 September 2021. MCD12C1 V6 dataset is available at <https://lpdaac.usgs.gov/products/mcd12c1v006/>, accessed on 22 September 2021.

**Acknowledgments:** We appreciate Zhu for providing leaf area index data. We appreciate global ecological modelers for providing Trendy-v6 DGVMs data.

**Conflicts of Interest:** The authors declare no conflict of interest.

## References

1. Dai, A. Increasing drought under global warming in observations and models. *Nat. Clim. Chang.* **2013**, *3*, 52–58. [\[CrossRef\]](#)
2. Scheffran, J.; Battaglini, A. Climate and conflicts: The security risks of global warming. *Reg. Environ. Chang.* **2011**, *11*, 27–39. [\[CrossRef\]](#)
3. Zheng, C.; Tang, X.; Gu, Q.; Wang, T.; Wei, J.; Song, L.; Ma, M. Climatic anomaly and its impact on vegetation phenology, carbon sequestration and water-use efficiency at a humid temperate forest. *J. Hydrol.* **2018**, *565*, 150–159. [\[CrossRef\]](#)
4. Allen, C.D.; Macalady, A.K.; Chenchouni, H.; Bachelet, D.; McDowell, N.; Vennetier, M.; Kitzberger, T.; Rigling, A.; Breshears, D.D.; Hogg, E.H.; et al. A global overview of drought and heat-induced tree mortality reveals emerging climate change risks for forests. *For. Ecol. Manag.* **2010**, *259*, 660–684. [\[CrossRef\]](#)
5. Lemordant, L.; Gentine, P.; Swann, A.S.; Cook, B.I.; Scheff, J. Critical impact of vegetation physiology on the continental hydrologic cycle in response to increasing CO<sub>2</sub>. *Proc. Natl. Acad. Sci. USA* **2018**, *115*, 4093–4098. [\[CrossRef\]](#) [\[PubMed\]](#)
6. Ogutu, B.O.; D’Adamo, F.; Dash, J. Impact of vegetation greening on carbon and water cycle in the African Sahel-Sudano-Guinean region. *Glob. Planet. Chang.* **2021**, *202*, 103524. [\[CrossRef\]](#)
7. Isbell, F.; Craven, D.; Connolly, J.; Loreau, M.; Schmid, B.; Beierkuhnlein, C.; Bezemer, T.M.; Bonin, C.; Bruelheide, H.; De Luca, E. Biodiversity increases the resistance of ecosystem productivity to climate extremes. *Nature* **2015**, *526*, 574–577. [\[CrossRef\]](#)
8. Mitchell, P.J.; O’Grady, A.P.; Pinkard, E.A.; Brodribb, T.J.; Arndt, S.K.; Blackman, C.J.; Duursma, R.A.; Fensham, R.J.; Hilbert, D.W.; Nitschke, C.R.; et al. An ecoclimatic framework for evaluating the resilience of vegetation to water deficit. *Glob. Chang. Biol.* **2016**, *22*, 1677–1689. [\[CrossRef\]](#)
9. Hossain, M.L.; Li, J. NDVI-based vegetation dynamics and its resistance and resilience to different intensities of climatic events. *Glob. Ecol. Conserv.* **2021**, *30*, e01768. [\[CrossRef\]](#)
10. Boulton, C.A.; Lenton, T.M.; Boers, N. Pronounced loss of Amazon rainforest resilience since the early 2000s. *Nat. Clim. Chang.* **2022**, *12*, 271–278. [\[CrossRef\]](#)
11. von Keyserlingk, J.; de Hoop, M.; Mayor, A.G.; Dekker, S.C.; Rietkerk, M.; Foerster, S. Resilience of vegetation to drought: Studying the effect of grazing in a Mediterranean rangeland using satellite time series. *Remote Sens. Environ.* **2021**, *255*, 112270. [\[CrossRef\]](#)
12. Jha, S.; Das, J.; Sharma, A.; Hazra, B.; Goyal, M.K. Probabilistic evaluation of vegetation drought likelihood and its implications to resilience across India. *Glob. Planet. Chang.* **2019**, *176*, 23–35. [\[CrossRef\]](#)
13. Sinha, J.; Sharma, A.; Khan, M.; Goyal, M.K. Assessment of the impacts of climatic variability and anthropogenic stress on hydrologic resilience to warming shifts in Peninsular India. *Sci. Rep.* **2018**, *8*, 13833. [\[CrossRef\]](#)
14. McDowell, N.; Pockman, W.T.; Allen, C.D.; Breshears, D.D.; Cobb, N.; Kolb, T.; Plaut, J.; Sperry, J.; West, A.; Williams, D.G.; et al. Mechanisms of plant survival and mortality during drought: Why do some plants survive while others succumb to drought? *New Phytol.* **2008**, *178*, 719–739. [\[CrossRef\]](#)
15. Verbesselt, J.; Umlauf, N.; Hirota, M.; Holmgren, M.; Van Nes, E.H.; Herold, M.; Zeileis, A.; Scheffer, M. Remotely sensed resilience of tropical forests. *Nat. Clim. Chang.* **2016**, *6*, 1028–1031. [\[CrossRef\]](#)
16. Bennett, A.C.; Dargie, G.C.; Cuni-Sanchez, A.; Tshibamba Mukendi, J.; Hubau, W.; Mukinzi, J.M.; Phillips, O.L.; Malhi, Y.; Sullivan, M.J.P.; Cooper, D.L.M.; et al. Resistance of African tropical forests to an extreme climate anomaly. *Proc. Natl. Acad. Sci. USA* **2021**, *118*, e2003169118. [\[CrossRef\]](#)
17. Piao, S.; Nan, H.; Huntingford, C.; Ciais, P.; Friedlingstein, P.; Sitch, S.; Peng, S.; Ahlström, A.; Canadell, J.G.; Cong, N. Evidence for a weakening relationship between interannual temperature variability and northern vegetation activity. *Nat. Commun.* **2014**, *5*, 5018. [\[CrossRef\]](#)
18. Huang, M.; Piao, S.; Ciais, P.; Peñuelas, J.; Wang, X.; Keenan, T.F.; Peng, S.; Berry, J.A.; Wang, K.; Mao, J. Air temperature optima of vegetation productivity across global biomes. *Nat. Ecol. Evol.* **2019**, *3*, 772–779. [\[CrossRef\]](#)
19. Sullivan, M.; Lewis, S.L.; Affum-Baffoe, K.; Castilho, C.; Phillips, O.L. Long-term thermal sensitivity of Earth’s tropical forests. *Science* **2020**, *368*, 869–874. [\[CrossRef\]](#)
20. Verhoeve, S.; Keijzer, T.; Kaitila, R.; Wickama, J.; Sterk, G. Vegetation Resilience under Increasing Drought Conditions in Northern Tanzania. *Remote Sens.* **2021**, *13*, 4592. [\[CrossRef\]](#)
21. Jiang, H.; Song, L.; Li, Y.; Ma, M.; Fan, L. Monitoring the Reduced Resilience of Forests in Southwest China Using Long-Term Remote Sensing Data. *Remote Sens.* **2021**, *14*, 32. [\[CrossRef\]](#)
22. Wu, J.; Liang, S. Assessing Terrestrial Ecosystem Resilience using Satellite Leaf Area Index. *Remote Sens.* **2020**, *12*, 595. [\[CrossRef\]](#)
23. Kang, W.; Liu, S.; Chen, X.; Feng, K.; Guo, Z.; Wang, T. Evaluation of ecosystem stability against climate changes via satellite data in the eastern sandy area of northern China. *J. Environ. Manag.* **2022**, *308*, 114596. [\[CrossRef\]](#)
24. Seddon, A.W.; Macias-Fauria, M.; Long, P.R.; Benz, D.; Willis, K.J. Sensitivity of global terrestrial ecosystems to climate variability. *Nature* **2016**, *531*, 229–232. [\[CrossRef\]](#) [\[PubMed\]](#)

25. Ivits, E.; Horion, S.; Erhard, M.; Fensholt, R. Assessing European ecosystem stability to drought in the vegetation growing season. *Glob. Ecol. Biogeogr.* **2016**, *25*, 1131–1143. [[CrossRef](#)]
26. Halpern, C.B. Early Successional Pathways and the Resistance and Resilience of Forest Communities. *Ecology* **1988**, *69*, 1703–1715. [[CrossRef](#)]
27. De Keersmaecker, W.; Lhermitte, S.; Tits, L.; Honnay, O.; Somers, B.; Coppin, P. A model quantifying global vegetation resistance and resilience to short-term climate anomalies and their relationship with vegetation cover. *Glob. Ecol. Biogeogr.* **2015**, *24*, 539–548. [[CrossRef](#)]
28. Zhu, Z.; Bi, J.; Pan, Y.; Ganguly, S.; Anav, A.; Xu, L.; Samanta, A.; Piao, S.; Nemani, R.R.; Myneni, R.B. Global Data Sets of Vegetation Leaf Area Index (LAI)3g and Fraction of Photosynthetically Active Radiation (FPAR)3g Derived from Global Inventory Modeling and Mapping Studies (GIMMS) Normalized Difference Vegetation Index (NDVI)3g for the Period 1981 to 2011. *Remote Sens.* **2013**, *5*, 927–948. [[CrossRef](#)]
29. Le Quéré, C.; Andrew, R.M.; Friedlingstein, P.; Sitch, S.; Pongratz, J.; Manning, A.C.; Korsbakken, J.I.; Peters, G.P.; Canadell, J.G.; Jackson, R.B. Global carbon budget 2017. *Earth Syst. Sci. Data* **2018**, *10*, 405–448. [[CrossRef](#)]
30. Park, H.; Jeong, S. Leaf area index in Earth system models: How the key variable of vegetation seasonality works in climate projections. *Environ. Res. Lett.* **2021**, *16*, 034027. [[CrossRef](#)]
31. Holben, B.N. Characteristics of maximum-value composite images from temporal AVHRR data. *Int. J. Remote Sens.* **1986**, *7*, 1417–1434. [[CrossRef](#)]
32. Gouveia, C.; DaCamara, C.; Trigo, R. Post-fire vegetation recovery in Portugal based on spot/vegetation data. *Nat. Hazards Earth Syst. Sci.* **2010**, *10*, 673–684. [[CrossRef](#)]
33. Wei, Y.; Liu, S.; Huntzinger, D.N.; Michalak, A.M.; Viovy, N.; Post, W.M.; Schwalm, C.R.; Schaefer, K.; Jacobson, A.R.; Lu, C. The North American carbon program multi-scale synthesis and terrestrial model intercomparison project—Part 2: Environmental driver data. *Geosci. Model. Dev.* **2014**, *7*, 2875–2893. [[CrossRef](#)]
34. Hurtt, G.C.; Chini, L.P.; Frolking, S.; Betts, R.; Feddema, J.; Fischer, G.; Fisk, J.; Hibbard, K.; Houghton, R.; Janetos, A. Harmonization of land-use scenarios for the period 1500–2100: 600 years of global gridded annual land-use transitions, wood harvest, and resulting secondary lands. *Clim. Chang.* **2011**, *109*, 117–161. [[CrossRef](#)]
35. Klein Goldewijk, K.; Beusen, A.; Doelman, J.; Stehfest, E. Anthropogenic land use estimates for the Holocene—HYDE 3.2. *Earth Syst. Sci. Data* **2017**, *9*, 927–953. [[CrossRef](#)]
36. Wu, D.; Piao, S.; Zhu, D.; Wang, X.; Ciais, P.; Bastos, A.; Xu, X.; Xu, W. Accelerated terrestrial ecosystem carbon turnover and its drivers. *Glob. Chang. Biol.* **2020**, *26*, 5052–5062. [[CrossRef](#)]
37. Harris, I.; Osborn, T.J.; Jones, P.; Lister, D. Version 4 of the CRU TS monthly high-resolution gridded multivariate climate dataset. *Sci. Data* **2020**, *7*, 109. [[CrossRef](#)]
38. Lionello, P.; Scarascia, L. The relation between climate change in the Mediterranean region and global warming. *Reg. Environ. Chang.* **2018**, *18*, 1481–1493. [[CrossRef](#)]
39. Du, L.; Mickle, N.; Zou, Z.; Huang, Y.; Shi, Z.; Jiang, L.; McCarthy, H.R.; Liang, J.; Luo, Y. Global patterns of extreme drought-induced loss in land primary production: Identifying ecological extremes from rain-use efficiency. *Sci. Total Environ.* **2018**, *628–629*, 611–620. [[CrossRef](#)]
40. Friedl, M.A.; Sulla-Menashe, D.; Tan, B.; Schneider, A.; Ramankutty, N.; Sibley, A.; Huang, X.M. MODIS Collection 5 global land cover: Algorithm refinements and characterization of new datasets. *Remote Sens. Environ.* **2010**, *114*, 168–182. [[CrossRef](#)]
41. Mu, B.; Zhao, X.; Wu, D.; Wang, X.; Zhao, J.; Wang, H.; Zhou, Q.; Du, X.; Liu, N. Vegetation Cover Change and Its Attribution in China from 2001 to 2018. *Remote Sens.* **2021**, *13*, 496. [[CrossRef](#)]
42. Wu, D.; Zhao, X.; Liang, S.; Zhou, T.; Huang, K.; Tang, B.; Zhao, W. Time-lag effects of global vegetation responses to climate change. *Glob. Chang. Biol.* **2015**, *21*, 3520–3531. [[CrossRef](#)] [[PubMed](#)]
43. Kern, A.; Marjanović, H.; Dobor, L.; Anić, M.; Hlásny, T.; Barcza, Z. Identification of years with extreme vegetation state in Central Europe based on remote sensing and meteorological data. *South-East Eur. For. SEEFOR* **2017**, *8*, 1–20. [[CrossRef](#)]
44. Wu, D.; Piao, S.; Liu, Y.; Ciais, P.; Yao, Y. Evaluation of CMIP5 Earth System Models for the Spatial Patterns of Biomass and Soil Carbon Turnover Times and Their Linkage with Climate. *J. Clim.* **2018**, *31*, 5947–5960. [[CrossRef](#)]
45. Watts, L.M.; Laffan, S.W. Effectiveness of the BFAST algorithm for detecting vegetation response patterns in a semi-arid region. *Remote Sens. Environ.* **2014**, *154*, 234–245. [[CrossRef](#)]
46. Zampieri, M.; Grizzetti, B.; Toreti, A.; De Palma, P.; Collalti, A.J.E.R.L. Rise and fall of vegetation annual primary production resilience to climate variability projected by a large ensemble of Earth System Models’ simulations. *Environ. Res. Lett.* **2021**, *16*, 105001. [[CrossRef](#)]
47. Hirota, M.; Holmgren, M.; Van Nes, E.H.; Scheffer, M. Global resilience of tropical forest and savanna to critical transitions. *Science* **2011**, *334*, 232–235. [[CrossRef](#)]
48. Scheffer, M.; Carpenter, S.R.; Dakos, V.; Van Nes, E. Generic Indicators of Ecological Resilience: Inferring the Chance of a Critical Transition. *Annu. Rev. Ecol. Evol. Syst.* **2015**, *46*, 145–167. [[CrossRef](#)]
49. Monge-González, M.L.; Guerrero-Ramírez, N.; Krömer, T.; Kreft, H.; Craven, D. Functional diversity and redundancy of tropical forests shift with elevation and forest-use intensity. *J. Appl. Ecol.* **2021**, *58*, 1827–1837. [[CrossRef](#)]
50. Nemani, R.R.; Keeling, C.D.; Hashimoto, H.; Jolly, W.M.; Piper, S.C.; Tucker, C.J.; Myneni, R.B.; Running, S.W. Climate-driven increases in global terrestrial net primary production from 1982 to 1999. *Science* **2003**, *300*, 1560–1563. [[CrossRef](#)]

51. Ciemer, C.; Boers, N.; Hirota, M.; Kurths, J.; Mueller-Hansen, F.; Oliveira, R.S.; Winkelmann, R.J.N.G. Higher resilience to climatic disturbances in tropical vegetation exposed to more variable rainfall. *Nat. Geosci.* **2019**, *12*, 174–179. [[CrossRef](#)]
52. Cole, L.E.; Bhagwat, S.A.; Willis, K.J. Recovery and resilience of tropical forests after disturbance. *Nat. Commun.* **2014**, *5*, 3906. [[CrossRef](#)]
53. Bagchi, S.; Briske, D.D.; Wu, X.; McClaran, M.P.; Bestelmeyer, B.T.; Fernández-Giménez, M.E.J.E.A. Empirical assessment of state-and-transition models with a long-term vegetation record from the Sonoran Desert. *Ecol. Appl.* **2012**, *22*, 400–411. [[CrossRef](#)]
54. Liu, D.; Zhang, C.; Ogaya, R.; Fernández-Martínez, M.; Pugh, T.A.M.; Peñuelas, J. Increasing climatic sensitivity of global grassland vegetation biomass and species diversity correlates with water availability. *New Phytol.* **2021**, *230*, 1761–1771. [[CrossRef](#)]
55. Wu, D.; Vargas, G.G.; Powers, J.S.; McDowell, N.G.; Becknell, J.M.; Perez-Aviles, D.; Medvigy, D.; Liu, Y.; Katul, G.G.; Calvo-Alvarado, J.C.; et al. Reduced ecosystem resilience quantifies fine-scale heterogeneity in tropical forest mortality responses to drought. *Glob. Chang. Biol.* **2022**, *28*, 2081–2094. [[CrossRef](#)]
56. Liu, Q.; Fu, Y.H.; Zeng, Z.; Huang, M.; Li, X.; Piao, S. Temperature, precipitation, and insolation effects on autumn vegetation phenology in temperate China. *Glob. Chang. Biol.* **2016**, *22*, 644–655. [[CrossRef](#)]
57. Wu, Z.; Dijkstra, P.; Koch, G.W.; Peñuelas, J.; Hungate, B.A. Responses of terrestrial ecosystems to temperature and precipitation change: A meta-analysis of experimental manipulation. *Glob. Chang. Biol.* **2011**, *17*, 927–942. [[CrossRef](#)]
58. Piao, S.; Liu, Z.; Wang, T.; Peng, S.; Ciais, P.; Huang, M.; Ahlstrom, A.; Burkhardt, J.F.; Chevallier, F.; Janssens, I.A. Weakening temperature control on the interannual variations of spring carbon uptake across northern lands. *Nat. Clim. Chang.* **2017**, *7*, 359–363. [[CrossRef](#)]
59. Chen, J.M.; Ju, W.; Ciais, P.; Viovy, N.; Liu, R.; Liu, Y.; Lu, X. Vegetation structural change since 1981 significantly enhanced the terrestrial carbon sink. *Nat. Commun.* **2019**, *10*, 4259. [[CrossRef](#)]
60. Piao, S.; Yin, G.; Tan, J.; Cheng, L.; Huang, M.; Li, Y.; Liu, R.; Mao, J.; Myneni, R.B.; Peng, S. Detection and attribution of vegetation greening trend in China over the last 30 years. *Glob. Chang. Biol.* **2015**, *21*, 1601–1609. [[CrossRef](#)]
61. Zhu, Z.; Piao, S.; Myneni, R.B.; Huang, M.; Zeng, Z.; Canadell, J.G.; Ciais, P.; Sitch, S.; Friedlingstein, P.; Arneeth, A.; et al. Greening of the Earth and its drivers. *Nat. Clim. Chang.* **2016**, *6*, 791–795. [[CrossRef](#)]
62. Wu, D.; Wu, H.; Zhao, X.; Zhou, T.; Tang, B.; Zhao, W.; Jia, K. Evaluation of spatiotemporal variations of global fractional vegetation cover based on GIMMS NDVI data from 1982 to 2011. *Remote Sens.* **2014**, *6*, 4217–4239. [[CrossRef](#)]
63. Wang, X.; Piao, S.; Ciais, P.; Friedlingstein, P.; Myneni, R.B.; Cox, P.; Heimann, M.; Miller, J.; Peng, S.; Wang, T. A two-fold increase of carbon cycle sensitivity to tropical temperature variations. *Nature* **2014**, *506*, 212–215. [[CrossRef](#)] [[PubMed](#)]